# Hollows on Mercury: MESSENGER Evidence for Geologically Recent Volatile-Related Activity

David T. Blewett, *et al.*

*Science* **333**, 1856 (2011);
DOI: 10.1126/science.1211681

28. K. J. Hon, J. Kauahikaua, R. Denlinger, K. Mackay, *Geol. Soc. Am. Bull.* **106**, 351 (1994).
29. L. R. Nittler *et al.*, *Science* **333**, 1847 (2011).
30. C. I. Fassett *et al.*, *Earth Planet. Sci. Lett.* **285**, 297 (2009).
31. H. Hiesinger, J. W. Head III, U. Wolf, R. Jaumann, G. Neukum, in *Recent Advances and Current Research Issues in Lunar Stratigraphy*, W. A. Ambrose, D. A. Williams, Eds. (Special Paper 477, Geological Society of America, Boulder, CO, 2011), pp. 1–51.

**Acknowledgments:** We thank the MESSENGER team for development and flight operations. The NASA Discovery Program supports the MESSENGER mission through contract NAS5-97271 to The Johns Hopkins University Applied Physics Laboratory and NASW-00002 to the Carnegie Institution of Washington.

**Supporting Online Material**
www.sciencemag.org/cgi/content/full/333/6051/1853/DC1
SOM Text
Figs. S1 to S3

1 August 2011; accepted 5 September 2011
10.1126/science.1211997

# Hollows on Mercury: MESSENGER Evidence for Geologically Recent Volatile-Related Activity

**David T. Blewett,[1]* Nancy L. Chabot,[1] Brett W. Denevi,[1] Carolyn M. Ernst,[1] James W. Head,[2] Noam R. Izenberg,[1] Scott L. Murchie,[1] Sean C. Solomon,[3] Larry R. Nittler,[3] Timothy J. McCoy,[4] Zhiyong Xiao,[5,6] David M. H. Baker,[2] Caleb I. Fassett,[2] Sarah E. Braden,[7] Jürgen Oberst,[8] Frank Scholten,[8] Frank Preusker,[8] Debra M. Hurwitz[2]**

High-resolution images of Mercury's surface from orbit reveal that many bright deposits within impact craters exhibit fresh-appearing, irregular, shallow, rimless depressions. The depressions, or hollows, range from tens of meters to a few kilometers across, and many have high-reflectance interiors and halos. The host rocks, which are associated with crater central peaks, peak rings, floors, and walls, are interpreted to have been excavated from depth by the crater-forming process. The most likely formation mechanisms for the hollows involve recent loss of volatiles through some combination of sublimation, space weathering, outgassing, or pyroclastic volcanism. These features support the inference that Mercury's interior contains higher abundances of volatile materials than predicted by most scenarios for the formation of the solar system's innermost planet.

The MESSENGER spacecraft entered orbit about Mercury on 18 March 2011, after which the Mercury Dual Imaging System (MDIS) (*1*) acquired high-spatial-resolution images. Many of the images reveal an unusual landform on Mercury, characterized by irregularly shaped, shallow, rimless depressions, commonly in clusters and in association with high-reflectance materials. Here, we describe this class of landform and its distribution and suggest that it indicates recent volatile-related activity.

MESSENGER is engaged in global imaging of Mercury's surface at a pixel dimension of ~250 m. As part of this mapping, targeted observations of selected areas are made using the MDIS, with pixel dimensions of ~10 m for monochrome imaging and 80 m for multispectral images. Resolution is greatest—more than a factor of 10 better than with standard mapping—for areas northward of 20° N, where the spacecraft orbit is closest to Mercury. Several of the targeted areas (Figs. 1, A and B) show depressions, or hollows, that are irregular in shape with generally rounded edges. Horizontal dimensions range from tens of meters to several kilometers. The hollows are shallow and rimless, and many have high-reflectance interiors and diffuse bright halos. The interiors are mostly smooth and flat, but some have small bumps, hills, or mesas, the tops of which may be remnants of the original surface. Many form clusters, although some are isolated. The hollows appear fresh and lack superposed impact craters, implying that they are relatively young.

To date, we have found hollows within impact craters that span a range of sizes. The examples in Fig. 1, A and B, are on impact crater central peaks or the peak rings of impact basins. Additional examples on basin peak rings are shown in Fig. 1, C and D. Similar high-reflectance hollows occur on the floors, walls, and rims of some medium-sized impact craters (Fig. 1, E and F). The hollows are found in comparatively fresh (Kuiperian) rayed craters, more degraded craters, and basins in a variety of states of erosion.

Craters such as Tyagaraja and Sander (Fig. 2, A and B) exhibit extensive fields of coalescing bright-interior/bright-halo hollows on their floors, lending an etched appearance to the terrain. The etched terrain on Tyagaraja's floor displays some of the highest reflectance on the planet (~2.5 times the global average), has a relatively shallow ("blue") spectral slope (*2*), and lacks clear spectral features in MDIS multispectral data. Surfaces with spectral properties such as those of the hollows in Figs. 1D and 2A were also seen in lower-spatial-resolution multispectral images from the Mariner 10 and MESSENGER flybys (*3*–*7*).

Materials with high reflectance and extremely blue color are global spectral outliers and have been termed "bright crater-floor deposits" (BCFDs) (*5*–*7*). MESSENGER flyby images indicated that BCFDs occur in several morphologic types, including varieties that have lobate outlines and those on central peaks and peak rings. Apart from Raditladi, Tyagaraja, and Sander (Figs. 1C and 2, A and B), prominent named examples include the deposits on the floors of the craters Balzac, de Graft, Kertesz, and Zeami and on the central peaks or peak rings of Eminescu and Vivaldi.

MESSENGER's orbital high-resolution and color imaging reveals that the areas identified as BCFDs are composed of hollows and etched terrain; hence, hollows are widespread across the planet (Fig. 3). Hollows have been found between ~66° N and 54° S and across all longitudes covered so far by orbital imaging. Many hollows occur in areas where there are exposures of low-reflectance material (LRM) (*5*, *6*), a major global color-compositional unit thought to have been originally emplaced at depth (*8*).

Volcanism, explosive outgassing, collapse into a subsurface void, and loss of volatile-rich material through sublimation are capable of creating irregularly shaped depressions on planetary surfaces. Volcanism was an important and widespread process on Mercury (*9*–*14*). Extrusive and explosive volcanism can produce rimless depressions in the form of calderas, vents, and collapse pits. A number of probable pyroclastic vents and deposits have been identified on Mercury (*12*, *13*, *15*–*17*). Also, an intrusive magmatic process has been proposed as the source for a class of pit craters on Mercury (*18*), via collapse after withdrawal of magma from a near-surface chamber. However, the size and morphology of the pyroclastic vents and pit craters identified to date on Mercury differ from those of the hollows. Most of the irregular depressions associated with pyroclastic deposits are large [several tens of kilometers (*16*, *17*)] relative to the hollows and typically occur as isolated depressions rather than in clusters. Moreover, the hollows occur on the tops and sides of central peak mountains as well as across impact crater walls and rims, which are unlikely locations for volcanic eruptions. The recognized pyroclastic deposits are associated with strong positive ("red") spectral slope across the visible and near-infrared (*5*, *6*, *15*–*17*) in contrast to the "blue" character of the hollows. Thus, if the

[1]The Johns Hopkins University Applied Physics Laboratory, Laurel, MD 20723, USA. [2]Department of Geological Sciences, Brown University, Providence, RI 02912, USA. [3]Department of Terrestrial Magnetism, Carnegie Institution of Washington, Washington, DC 20015, USA. [4]Smithsonian Institution, Washington, DC 20013, USA. [5]Lunar and Planetary Laboratory, University of Arizona, Tucson, AZ 85721, USA. [6]Faculty of Earth Sciences, China University of Geosciences, Wuhan, Hubei, 430074, P. R. China. [7]School of Earth and Space Exploration, Arizona State University, Tempe, AZ 85251, USA. [8]Institute of Planetary Research, German Aerospace Center, D-12489 Berlin, Germany.

*To whom correspondence should be addressed. E-mail: david.blewett@jhuapl.edu

hollows and etched terrain are products of volcanism, it must be a form that is physically and compositionally different from that which produced the recognized pyroclastic vents and deposits. In some cases, such as Praxiteles and Tyagaraja (Figs. 1D and 2A), the blue materials are found together with red materials.

Episodic minor explosive release of gas with no ejected juvenile material, as was proposed for an unusual lunar feature [Ina (*19*)], could disrupt the country rock and maintain a fresh, high-albedo surface against space weathering by solar wind and micrometeoroid bombardment. However, energetic outgassing alone may not account for the differences in color between the hollows and ordinary immature local materials (*20*). Fumarolic deposition and chemical alteration (*3*) were suggested as the origin of the bright, blue patches first observed in Mariner 10 images. The location of hollows and etched terrain within impact craters is consistent with the idea that deep-seated gases gain access to the surface along impact-induced fractures (*3*).

The association of hollows with impact craters and basins indicates a link with material that has been brought near or to the surface from depth. For example, the peak rings of the 170-km-diameter basin in Fig. 1A originated at depths of ~14 to 20 km (*21*), whereas the walls and ejecta of the crater in Fig. 1E probably were derived from depths of $\lesssim$2 km. Whether the material associated with the hollows is derived from greater or shallower depths, it could be that a component is unstable when it experiences the low-pressure, high-temperature environment of the surface or shallow subsurface, leading to sublimation and subsequent collapse. The example in Fig. 1F is instructive. The crater is at a high northern latitude. High-reflectance material is present on the upper portion of the northern wall, and several bright-halo hollows are located in a slump in the middle of the wall. Solar heating would be maximal on these south-facing surfaces, suggesting that development of the hollows and associated bright material is correlated with peaks in diurnal temperature. The steep slopes on the crater wall and slump should promote mass-wasting movement and continuously expose new material, so the bright material and hollows are likely to be young features.

The hollows share morphological similarities with portions of the "Swiss-cheese" terrain

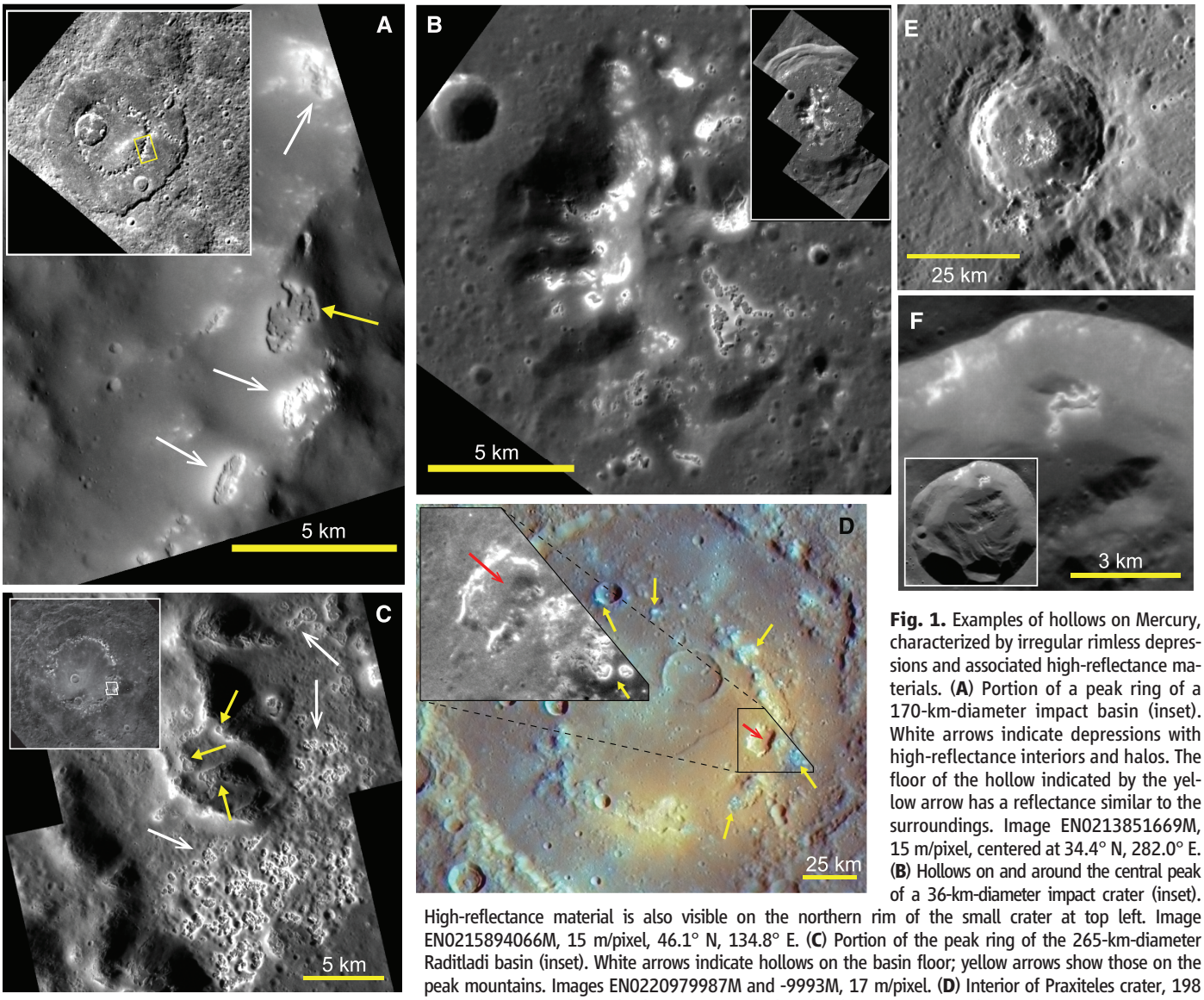


**Fig. 1.** Examples of hollows on Mercury, characterized by irregular rimless depressions and associated high-reflectance materials. (**A**) Portion of a peak ring of a 170-km-diameter impact basin (inset). White arrows indicate depressions with high-reflectance interiors and halos. The floor of the hollow indicated by the yellow arrow has a reflectance similar to the surroundings. Image EN0213851669M, 15 m/pixel, centered at 34.4° N, 282.0° E. (**B**) Hollows on and around the central peak of a 36-km-diameter impact crater (inset). High-reflectance material is also visible on the northern rim of the small crater at top left. Image EN0215894066M, 15 m/pixel, 46.1° N, 134.8° E. (**C**) Portion of the peak ring of the 265-km-diameter Raditladi basin (inset). White arrows indicate hollows on the basin floor; yellow arrows show those on the peak mountains. Images EN0220979987M and -9993M, 17 m/pixel. (**D**) Interior of Praxiteles crater, 198 km in diameter. Enhanced-color image in which red-to-blue variations indicate relative color; the green channel is a measure of overall albedo (*34*). Hollows (yellow arrows) appear bright blue; the large depression (red arrow) is a likely volcanic vent and the source of the reddish pyroclastic deposit. Inset is image EN0211416219M (53 m/pixel), showing details of the bright depressions. (**E**) High-reflectance depressions on the floor, walls, and rim of a partially degraded 25-km-diameter impact crater. Image EN0213154023M, 149 m/pixel, 23.3° N, 179.4° E. (**F**) Portion of a morphologically fresh 15-km-diameter crater (inset) with bright material on the upper wall and hollows on a wall slump. Image EN0218374376M, 18 m/pixel, 66.5° N, 153.2° E.

found in the south polar region of Mars (fig. S1): elongated, rounded depressions with flat floors that occur in spatially extensive groups similar to those in Raditladi, Tyagaraja, and Sander (Figs. 1C and 2, A and B). The martian terrain is produced by sublimation of $CO_2$ ice (*22*). The resemblance suggests that a sublimation process may be responsible for formation of the hollows.

Rather than via a temperature or pressure effect, the hollows on Mercury could form through degradation of a component susceptible to space weathering (by micrometeoroid bombardment and/or solar-wind sputtering). Impact vaporization followed by sputtering of sulfide minerals has been invoked (*23*, *24*) to explain the deficit of sulfur measured at the surface of asteroid Eros by the Near Earth Asteroid Rendezvous-Shoemaker spacecraft's x-ray spectrometer (*25*). The MESSENGER X-Ray Spectrometer has found a surprisingly high abundance of sulfur in Mercury's regolith (*26*). Whatever the identity of the sputtered or sublimated material, hollows lacking high-reflectance halos or interiors (Fig. 1A) could be inactive, resulting from exhaustion of the volatile-bearing phase or development of a protective lag, whereas the nearby depressions with bright interiors and halos probably are sites of current activity.

Other volatile elements or compounds could be involved in formation of the hollows. For example, large volcanic eruptions that occurred

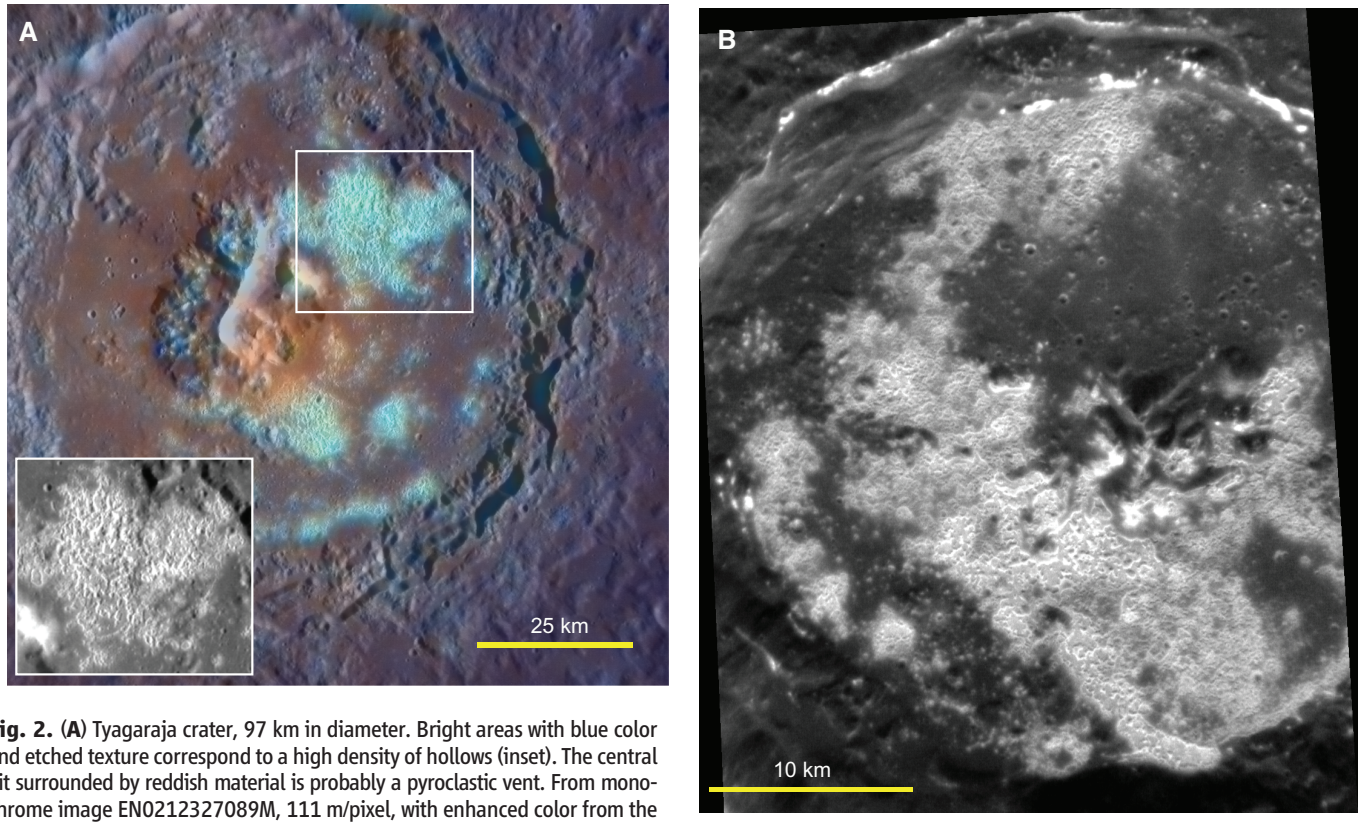


**Fig. 2.** (**A**) Tyagaraja crater, 97 km in diameter. Bright areas with blue color and etched texture correspond to a high density of hollows (inset). The central pit surrounded by reddish material is probably a pyroclastic vent. From monochrome image EN0212327089M, 111 m/pixel, with enhanced color from the eight-filter set EW0217266882I (*34*). (**B**) Sander crater, 47 km in diameter. A high density of hollows occurs in the high-reflectance portions of the crater floor; others are found on the northern crater rim and wall terraces. Stereo analysis (*35*) indicates that any elevation differences between the high-reflectance and darker areas of the floor are ≲20 m. Image EN0218289182M, 30 m/pixel.

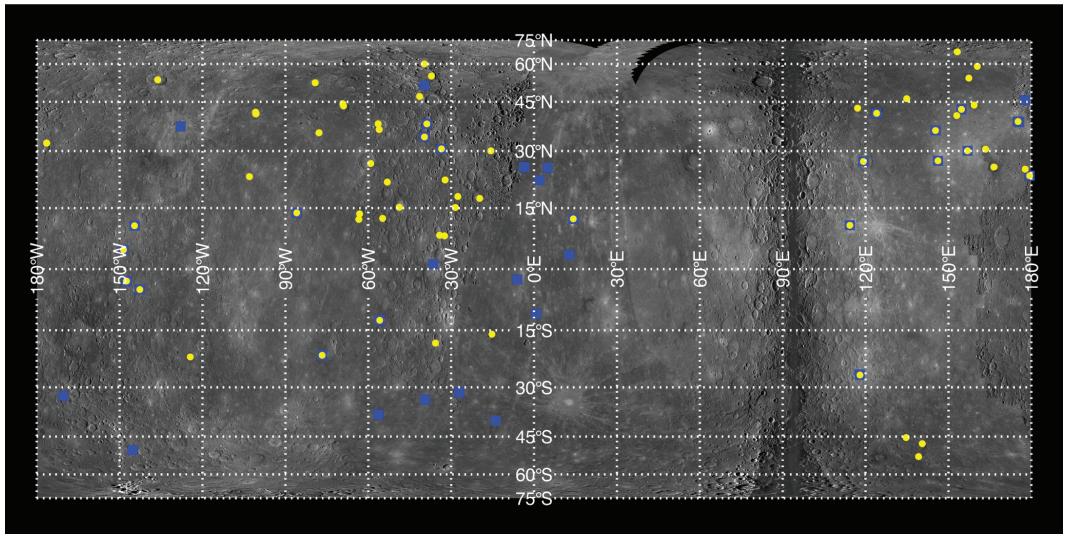


**Fig. 3.** Global distribution (simple cylindrical projection) of hollows seen at high spatial resolution (yellow dots) and materials with high reflectance and strong blue color (BCFDs, blue squares). Some portions of the planet have not yet been imaged at high resolution with illumination and viewing conditions best suited for morphological or color analysis (supporting online material text).

when the surface was below the sublimation temperature (that is, at night) may have produced volatile-rich deposits when magmatic gases or fumarolic minerals condensed onto the cold surroundings. These materials could then have been sequestered through burial by extensive thicknesses of pyroclastic deposits or lava. Subsequent impact cratering could have exhumed these materials to the shallow subsurface, followed by formation of depressions by scarp retreat as the volatile component sublimated.

To estimate the rate at which hollows may be forming, we used shadow-length measurements to determine the average depth of the hollows on the floor of the Raditladi basin (Fig. 1C). This value (44 m), combined with the age of the basin as constrained by the crater size-frequency distribution [$10^9$ years (*27*)] yields an erosion rate of 0.04 μm/year, or 1 cm in 200,000 years, under the assumption that erosion proceeds only downwards. In many areas, however, the flat floors and rounded outlines suggest that the hollows are enlarged through radial growth—down to a resistant base, then laterally by scarp retreat. We determined the characteristic average radius (137 m) for isolated hollows and individual hollows that form merged groups on the floor of Raditladi. Under strictly radial growth, the erosion rate is 0.14 μm/year, or 1 cm in 70,000 years. For comparison, estimates for the rate of scarp retreat in the martian "Swiss-cheese" terrain are ~1 m per Earth year (*22*), and the rate of abrasion of kilogram-sized lunar rocks by micrometeoroid bombardment is ~1 cm per $10^7$ years (*28*). Although the uncertainties in the formation rate are large, the existence on Mercury of a process modifying the terrain faster than lunar micrometeoroid erosion but more slowly than martian $CO_2$ ice sublimation can account for why the hollows appear to be much younger than the impact structures in which they are found.

The involvement of volatiles in candidate formation mechanisms for the hollows fits with growing evidence (*16*, *17*, *26*, *29*) that Mercury's interior contains higher abundances of volatile elements than are predicted by several planetary formation models for the innermost planet (*30*–*32*). Mercury is a small rocky-metal world whose internal geological activity was generally thought to have ended long ago. The presence of potentially recent surface modification implies that Mercury's nonimpact geological evolution may still be ongoing.

### References and Notes


1. S. E. Hawkins III *et al.*, *Space Sci. Rev.* **131**, 247 (2007).
2. Mercury's surface reflectance spectrum has a positive slope from ultraviolet to near-infrared wavelengths. Spectral slopes less steep than the global average are said to be "blue," and those with greater slopes are termed "red." The reflectance in 559-nm filter images is 0.140 for the hollows on Tyagaraja's floor versus 0.057 for the Mercury global average. The normalized 559-nm reflectance was measured for the continuous ejecta of 23 rayed (Kuiperian) craters and 20 BCFDs. For the Kuiperian craters, the mean reflectance is 0.09 ± 0.01. For the BCFDs, the mean reflectance is 0.107 ± 0.018.
3. D. Dzurisin, *Geophys. Res. Lett.* **4**, 383 (1977).
4. B. Rava, B. Hapke, *Icarus* **71**, 397 (1987).
5. M. S. Robinson *et al.*, *Science* **321**, 66 (2008).
6. D. T. Blewett *et al.*, *Earth Planet. Sci. Lett.* **285**, 272 (2009).
7. D. T. Blewett *et al.*, *Icarus* **209**, 239 (2010).
8. B. W. Denevi *et al.*, *Science* **324**, 613 (2009).
9. R. G. Strom, N. J. Trask, J. E. Guest, *J. Geophys. Res.* **80**, 2478 (1975).
10. P. D. Spudis, J. E. Guest, in *Mercury*, F. Vilas, C. R. Chapman, M. S. Matthews, Eds. (Univ. of Arizona Press, Tucson, AZ, 1988), pp. 118–164.
11. M. S. Robinson, P. G. Lucey, *Science* **275**, 197 (1997).
12. J. W. Head *et al.*, *Science* **321**, 69 (2008).
13. J. W. Head *et al.*, *Earth Planet. Sci. Lett.* **285**, 227 (2009).
14. J. W. Head *et al.*, *Science* **333**, 1853 (2011).
15. S. L. Murchie *et al.*, *Science* **321**, 73 (2008).
16. L. Kerber *et al.*, *Earth Planet. Sci. Lett.* **285**, 263 (2009).
17. L. Kerber *et al.*, *Planet. Space Sci.*, 8 April 2011 (10.1016/j.pss.2011.03.020).
18. J. J. Gillis-Davis *et al.*, *Earth Planet. Sci. Lett.* **285**, 243 (2009).
19. P. H. Schultz, M. I. Staid, C. M. Pieters, *Nature* **444**, 184 (2006).
20. Fresh (immature) materials in young crater ejecta and rays have spectral slopes that are less steep ("bluer") than the global average. However, the BCFDs have more extreme blue color (*5*, *6*).
21. The minimum depth of excavation of the central peak material is assumed to be the maximum depth of impact melting, which was estimated with methods described earlier (*33*).
22. M. C. Malin, M. A. Caplinger, S. D. Davis, *Science* **294**, 2146 (2001).
23. A. Kracher, D. W. G. Sears, *Icarus* **174**, 36 (2005).
24. M. J. Loeffler, C. A. Dukes, W. Y. Chang, L. A. McFadden, R. A. Baragiola, *Icarus* **195**, 622 (2008).
25. L. R. Nittler *et al.*, *Meteorit. Planet. Sci.* **36**, 1673 (2001).
26. L. R. Nittler *et al.*, *Science* **333**, 1847 (2011).
27. R. G. Strom, C. R. Chapman, W. J. Merline, S. C. Solomon, J. W. Head III, *Science* **321**, 79 (2008).
28. D. G. Ashworth, Lunar and planetary impact erosion, in *Cosmic Dust*, J. A. M. McDonnell, Ed. (Wiley, Hoboken, NJ, 1977), pp. 427–526.
29. P. N. Peplowski *et al.*, *Science* **333**, 1850 (2011).
30. J. S. Lewis, *Annu. Rev. Phys. Chem.* **24**, 339 (1973).
31. B. Fegley Jr., A. G. W. Cameron, *Earth Planet. Sci. Lett.* **82**, 207 (1987).
32. W. W. Benz, W. L. Slattery, A. G. W. Cameron, *Icarus* **74**, 516 (1988).
33. C. M. Ernst *et al.*, *Icarus* **209**, 210 (2010).
34. During orbital mapping, the MDIS wide-angle camera collects images through filters with central wavelengths of 430, 480, 559, 629, 749, 829, 898, and 997 nm. Red–green–blue presentation is the inverse of principal component two (iPC2)–PC1–(430-nm/629-nm ratio) (*5*, *8*).
35. F. Preusker *et al.*, *Planet. Space Sci.*, 28 July 2011 (10.1016/j.pss.2011.07.005).


**Acknowledgments:** This work was supported by NASA through the MESSENGER project and by a Participating Scientist grant to D.T.B. M. Robinson offered helpful comments on the manuscript. We thank N. Fontanella, S. Peel, E. Zhong, P. Pashai, and E. Coman for assistance with data processing and compilation. MESSENGER data are archived with the NASA Planetary Data System.

### Supporting Online Material

www.sciencemag.org/cgi/content/full/333/6051/1856/DC1
SOM Text
Fig. S1

25 July 2011; accepted 5 September 2011
10.1126/science.1211681

# The Global Magnetic Field of Mercury from MESSENGER Orbital Observations

**Brian J. Anderson,[1]* Catherine L. Johnson,[2,3] Haje Korth,[1] Michael E. Purucker,[4] Reka M. Winslow,[2] James A. Slavin,[5] Sean C. Solomon,[6] Ralph L. McNutt Jr.,[1] Jim M. Raines,[5] Thomas H. Zurbuchen[5]**

Magnetometer data acquired by the MESSENGER spacecraft in orbit about Mercury permit the separation of internal and external magnetic field contributions. The global planetary field is represented as a southward-directed, spin-aligned, offset dipole centered on the spin axis. Positions where the cylindrical radial magnetic field component vanishes were used to map the magnetic equator and reveal an offset of 484 ± 11 kilometers northward of the geographic equator. The magnetic axis is tilted by less than 3° from the rotation axis. A magnetopause and tail-current model was defined by using 332 magnetopause crossing locations. Residuals of the net external and offset-dipole fields from observations north of 30°N yield a best-fit planetary moment of 195 ± 10 nanotesla-$R_M^3$, where $R_M$ is Mercury's mean radius.

Mercury and Earth are the only terrestrial planets with global magnetic fields of internal origin, but Mercury's field is weak compared with Earth's (*1*–*3*). Explaining the comparatively weak field at Mercury with an Earth-like magnetic dynamo in the fluid outer core has proven challenging (*4*), and innovative theoretical solutions have been proposed (*5*, *6*) that can potentially be distinguished by the field geometry. Magnetometer observations made during Mercury flybys by the Mariner 10 (*1*) and MESSENGER (*2*, *3*) spacecraft indicate that the planet's internal field is consistent with an axially aligned dipole displaced northward by ~0.16 $R_M$, where $R_M$ is Mercury's mean radius, 2440 km. However, because of limited geographical coverage afforded by the flybys, the estimated dipole and quadrupole coefficients were highly correlated (*7*, *8*) such that the solutions were not unique. Moreover, signatures of plasma pressure near the equator raised questions about the field magnitudes recorded near the equator, implying that the inferred offset could have been the

[1]The Johns Hopkins University Applied Physics Laboratory, Laurel, MD 20723, USA. [2]University of British Columbia, Vancouver, BC V6T 1Z4, Canada. [3]Planetary Science Institute, Tucson, AZ 85719, USA. [4]Goddard Space Flight Center, Greenbelt, MD 20771, USA. [5]Department of Atmospheric, Oceanic and Space Sciences, University of Michigan, Ann Arbor, MI 48109, USA. [6]Department of Terrestrial Magnetism, Carnegie Institution of Washington, Washington, DC 20015, USA.

*To whom correspondence should be addressed. E-mail: brian.anderson@jhuapl.edu